Feedforward Neural Network for Orientation Estimation Under Magnetic and Acceleration Disturbances

Akos Odry[1*], Istvan Kecskes[2], Richard Pesti[1], Dominik Csik[1], Massimo Stefanoni[3], Imre Kovacs[1], Edit Laufer[4], Peter Sarcevic[1]

[1] Faculty of Engineering, University of Szeged, Mars tér 7, 6724 Szeged, Hungary, {odrya, pestir, csikd, kovacs.imre, sarcevic}@mk.u-szeged.hu

[2] Institute of Informatics, University of Dunaújváros, Táncsics Mihály u. 1, 2400 Dunaújváros, Hungary, kecskesi@uniduna.hu

[3] Doctoral School of Applied Informatics and Applied Mathematics, Óbuda University, Bécsi út 96/B, 1034 Budapest, Hungary, massimo.stefanoni@uni-obuda.hu

[4] Bánki Donát Faculty of Mechanical and Safety Engineering, Óbuda University, Bécsi út 96/B, 1034 Budapest, Hungary, laufer.edit@bgk.uni-obuda.hu

Abstract: Orientation estimation using magnetic, angular rate, and gravity (MARG) sensors is primarily affected by two error sources: external accelerations and magnetic disturbances. These disturbances hinder the accurate separation of sensor observations from their corresponding reference vectors, thereby degrading estimation accuracy. This paper presents a feedforward neural network (FFNN) architecture designed to estimate the disturbance vectors, enabling the generation of disturbance-compensated signals for improved state estimation within an Extended Kalman Filter (EKF) framework. First, the MARG sensor models are introduced and their integration into an EKF-based orientation estimation system is outlined. The proposed FFNN model for disturbance estimation is described in detail, with emphasis on its architectural design and the methodology for effective augmentation of the EKF. The practical feasibility of the approach is demonstrated in a laboratory setting using a calibrated UR5 robot. The robot performs various motions with a MARG sensor mounted on its end-effector, thereby subjecting the system to a range of disturbance magnitudes. A comprehensive evaluation is conducted across 16 distinct measurement scenarios, analyzing the influence of various disturbance combinations and intensities on estimation performance. The results indicate that the proposed FFNN-EKF approach consistently outperforms the standard EKF, with improvements in estimation accuracy ranging from 19% to 49%. This demonstrates the effectiveness of NN-based disturbance compensation in enhancing orientation estimation under real-world conditions.

Keywords: magnetic disturbance compensation; acceleration compensation; orientation estimation; neural network; Kalman filter

1 Introduction

Reliable orientation estimation is fundamental in embedded systems across robotics, mechatronics, automotive, aerospace, and human motion tracking applications [1]-[11].

MARG units, composed of accelerometers, gyroscopes, and magnetometers, are widely used for this task due to their lightweight, low cost, and high-resolution output. However, each sensor has inherent limitations: accelerometers measure both the gravitational acceleration and any additional acceleration caused by the movement of the body they are attached to; gyroscopes suffer from drift, and magnetometers are sensitive to magnetic disturbances. These issues hinder robust attitude estimation and require advanced algorithms [12]-[15].

Accurate orientation is essential for separating gravity and external acceleration components; if not ensured, velocity and position estimates accumulate large drift [16]-[18]. While EKFs are popular for incorporating system models [11], [19], [20], complementary filters (CFs) offer simpler, real-time alternatives [21], [22], though with less flexibility. In either case, effective handling of disturbances typically requires additional augmentation.

Existing compensation methods include constraint augmentation [11], gradient descent correction [22], measurement criteria-based sensor selection [20], adaptive covariance tuning [16], [23], [24], and soft computing approaches [25]. Most of the disturbance handling algorithms rely on covariance adjustment instead of explicit disturbance estimation. When exact disturbance vectors are required, either model-based [26], [27] or data-driven [5], [28]-[34] methods are used—both with notable drawbacks: high modeling effort or computational cost.

This paper introduces a novel methodology that employs a FFNN model for effective disturbance estimation and proposes its integration EKF framework. The goal is to enable orientation estimation using disturbance-compensated MARG sensor signals. To evaluate the real-world performance of the approach, a robotic arm-based laboratory setup is used, in which the impact of varying levels and combinations of external disturbances on EKF-based orientation estimation is systematically analyzed. The proposed FFNN-based real-time disturbance compensation method is then validated, demonstrating that the FFNN-EKF system significantly enhances orientation estimation accuracy under challenging and disturbance-prone conditions.

2 Problem Formulation

2.1 MARG Signals

In practice, measurements are affected by typical sensor errors: scale factor (ΔS), misalignment (M), temperature-dependent bias (ω_0, a_0, h_0, which evolves as random walks), white noise (η), and magnetic disturbances (soft iron B_{si}, hard iron b_{hi}) [1]:

$$\begin{aligned}
\Omega_k &= (I + \Delta S_\Omega) M_\Omega \omega_k + \omega_{0,k} + \eta_k^\Omega \\
\mathrm{A}_k &= (I + \Delta S_\mathrm{A}) M_\mathrm{A} \left(\alpha_k + {}^S g_k\right) + a_{0,k} + \eta_k^\mathrm{A} \\
\mathrm{H}_k &= (I + \Delta S_\mathrm{H}) M_\mathrm{H} (B_{si} h_k + b_{hi}) + h_{0,k} + \eta_k^\mathrm{H} \\
\omega_{0,k} &= \omega_{0,k-1} + \eta_k^{\omega_0} \\
\mathrm{a}_{0,k} &= a_{0,k-1} + \eta_k^{a_0} \\
\mathrm{h}_{0,k} &= h_{0,k-1} + \eta_k^{h_0}
\end{aligned} \tag{1}$$

where η^{ω_0}, η^{a_0}, η^{h_0} are zero-mean Gaussian noises. In-field calibration can compensate for these errors [35], enabling the use of corrected measurements ω_k, $\alpha_k + {}^S g_k$, and h_k for orientation estimation. However, accurate estimation is only guaranteed under quasi-static or constant velocity conditions ($\alpha_k \approx 0$) and in magnetic-free environments.

2.2 Sensor Fusion

Most MARG-based orientation estimation algorithms output a unit quaternion $q \in \mathbb{R}^4, \|q\| = 1$ representing the Earth frame's orientation relative to the sensor frame. EKF's motion model propagates the quaternion state using the numerical integration of angular rates, incorporating slowly varying gyroscope bias into the state vector: $x_k = \left(q_k, \omega_{0,k}\right)^T \in \mathbb{R}^7$ [25]. The prediction step is given by:

$$\begin{aligned}
q_{k+1} &= q_k + \tfrac{T_s}{2} \varrho(q_k) \begin{pmatrix} 0 \\ \Omega_k - \omega_{0,k} \end{pmatrix} + \eta_k^q \\
\omega_{0,k+1} &= \omega_{0,k} + \eta_k^{\omega_0}
\end{aligned} \tag{2}$$

where T_s is the sampling time, $\varrho(q_k)$ denotes the quaternion matrix, and η_k^q, $\eta_k^{\omega_0}$ represent the process noises. This defines the nonlinear state-space model $x_{k+1} = f(x_k, u_k, w_k)$, with $u_k = \Omega_k$ and $w_k = \left(\eta_k^q, \eta_k^{\omega_0}\right)$.

EKF's observation model prevents drift from open-loop propagation; it updates the state using accelerometer and magnetometer data. Assuming no external

disturbances, the reference vectors ${}^{E}g$ and ${}^{E}h$ are transformed to the sensor frame via the rotation matrix ${}^{S}_{E}R(q_k)$:

$$A_k = {}^{S}_{E}R(q_k)\ {}^{E}g, \tag{3}$$
$$H_k = {}^{S}_{E}R(q_k)\ {}^{E}h.$$

The rotation matrix is constructed using orthonormal triads from normalized sensor and reference vectors [36]:

$$M_k = [A_k, \quad A_k \times H_k, \quad A_k \times A_k \times H_k]$$
$${}^{E}M_k = [{}^{E}g, \quad {}^{E}g \times {}^{E}h, \quad {}^{E}g \times {}^{E}g \times {}^{E}h] \tag{4}$$
$${}^{S}_{E}R(q_k) = M_k\ {}^{E}M_k^T$$

A quaternion update $\tilde{q}_k$ is derived from equation (4), which is valid only under low dynamics and undisturbed magnetic conditions. This leads to a linear observation model: $y_k = G\ x_k + \eta_k^Q, G = [I_4, \quad 0_3]$, where η_k^Q reflects the uncertainty in $\tilde{q}_k$, increasing with external accelerations or magnetic interference.

External acceleration α_k is obtained outside the EKF using the current quaternion estimate $\hat{q}_k$ [16]:

$$\alpha_k = {}^{E}A_k - {}^{E}g, \quad \begin{pmatrix} 0 \\ {}^{E}A_k \end{pmatrix} = \hat{q}_k \otimes \begin{pmatrix} 0 \\ A_k \end{pmatrix} \otimes \hat{q}_k^*, \tag{5}$$

where $\hat{q}_k^*$ is the quaternion conjugate and $\otimes$ denotes quaternion multiplication.

The full EKF algorithm works as follows [37], [38]. Prediction: produces the a priori estimate $\hat{x}_{k+1}^-$ and covariance P_{k+1}^- using the process noise covariance $Q = \text{blkdiag}(\sigma^q I_4, \sigma^{\omega_0} I_3)$. Update: refines the estimate with measurement noise covariance $R = \sigma^Q I_4$. σ^q, σ^{ω_0}, and σ^Q define the noise variances for quaternion propagation, gyro bias, and observation, respectively. This standard EKF approach used for orientation estimation is clearly defined by equations (1)-(4), representing a widely adopted and well-established configuration in robotics and human motion applications [16], [25].

3 Disturbance Compensation

3.1 Method

The proposed approach focuses on identifying and compensating for disturbance vectors, thereby improving MARG measurement quality in orientation estimation, see Figure 1.

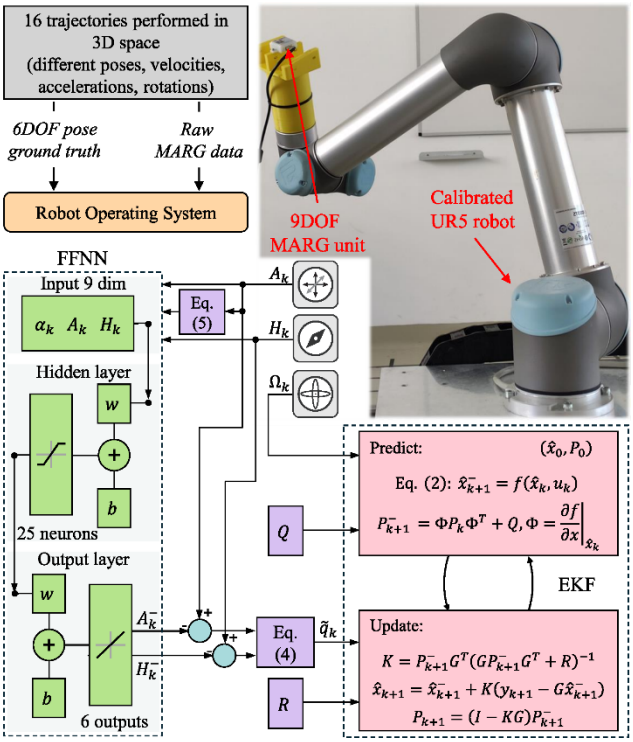

Figure 1
The method and experimental setup

The system uses a calibrated UR5 robot with a 9DOF MARG sensor mounted on the end-effector, delivering 100 Hz raw data. The UR5 executes a range of motions – from quasi-static to highly dynamic – controlled via the Robot Operating System (ROS). The MARG sensor is intentionally mounted on a relatively long fixture to ensure sufficient distance from the end effector and minimize disturbances, and the test scenarios are similarly designed to avoid close proximity to the robot's actuators.

UR5-based feedback provides ground truth for the MARG's pose, velocity, and acceleration, thereby a diverse dataset of motion scenarios is generated. The recorded dataset is used to design and train NN for providing correction vectors (A_k^-, H_k^-) in the orientation estimation problem. Multiple NN architectures are evaluated, varying in input combinations, hidden layer configurations, and neuron counts. The most efficient NN is integrated into the EKF orientation estimation loop. Performance is evaluated across a spectrum of scenarios – from static, undisturbed conditions to dynamic, noisy environments. The result is the identification of the most robust NN-EKF combination for reliable orientation estimation.

The ground truth-based correction targets $A_k^{-,target}$ and $H_k^{-,target}$ are computed from the true orientation q_k^{true} and constant reference vectors ${}^E g$ and ${}^E h$ as follows.

$$\begin{pmatrix} 0 \\ A_k^{-,target} \end{pmatrix} = \begin{pmatrix} 0 \\ A_k \end{pmatrix} - q_k^{true,*} \otimes \begin{pmatrix} 0 \\ {}^E g \end{pmatrix} \otimes q_k^{true} \tag{6}$$

$$\begin{pmatrix} 0 \\ H_k^{-,target} \end{pmatrix} = \begin{pmatrix} 0 \\ H_k \end{pmatrix} - q_k^{true,*} \otimes \begin{pmatrix} 0 \\ {}^E h \end{pmatrix} \otimes q_k^{true}$$

3.2 FFNN-EKF Framework

A comprehensive evaluation identified FFNN as the most suitable topology for disturbance estimation model, due to its simplicity, computational efficiency, and sufficient modeling capability [1].

The FFNN, trained with Levenberg-Marquardt backpropagation, was used to estimate six correction signals (accelerometer and magnetometer corrections along X, Y, and Z axes), and overfitting was evaluated via performance differences between training and test sets. A hidden layer size of 25 neurons was found to offer a good balance between accuracy and computational cost. The computational complexity analysis was presented in detail in [1]; it quantified the number of FLOPs, the constants characterizing the NN, and the implementation-specific constraints. Using MATLAB NN support tools, it was found that generating the compensation signals required 881 floating-point operations, and the overall computational complexity of the FFNN-EKF was 23% lower than that of the baseline EKF algorithm.

Input channel analysis showed that the best performance is provided with accelerometer, magnetometer, and approximated acceleration signals (A_k, H_k, α_k). This is attributed to the FFNN's explicit compensation of acceleration, vibration, and magnetic disturbances, yielding corrected signals for accurate quaternion-based orientation estimation.

Figure 1 presents the structure of the proposed FFNN-EKF framework. The system takes MARG measurements as inputs, specifically the real-time signals A_k, H_k, and α_k, which are processed by the FFNN to generate correction outputs A_k^- and H_k^-. These outputs effectively mitigate acceleration and magnetic disturbances, resulting in corrected signals that are suitable for use in the quaternion update step, as described in equation (4). During the prediction step of the EKF, the angular velocity input Ω_k is used to propagate the state, while in the update step, the refined quaternion $\tilde{q}_k$ adjusts the state estimate.

4 Experimental Results

4.1 Scenarios

The established laboratory environment executed 16 different measurement scenarios.

Tables 1 and 2 summarize the main characteristics of each scenario; these highlight the length and volume of each trajectory, the executed speed range and angular velocity measures. The total RPY change represents the cumulative absolute change in roll, pitch, and yaw angles throughout the entire trajectory, which well characterizes the executed rotational dynamics.

Table 1
Characteristics of the executed scenarios based on ground truth data

Scen.	Path length (m)	Volume (m^3)	Avg. speed (m/s)	Max speed (m/s)	Total RPY change (rad)
1	8.319	0.075	0.124	0.386	16.571
2	9.069	0.116	0.154	0.389	19.781
3	10.159	0.143	0.164	0.560	25.683
4	12.795	0.146	0.214	0.645	37.971
5	13.886	0.203	0.238	0.933	44.142
6	15.948	0.144	0.267	0.954	50.786
7	18.596	0.343	0.308	1.233	68.612
8	23.851	0.289	0.373	1.590	88.174
9	6.526	0.065	0.130	0.395	19.777
10	6.914	0.065	0.131	0.438	22.173
11	7.733	0.084	0.153	0.497	27.414
12	9.038	0.076	0.178	0.716	30.442
13	10.745	0.121	0.210	0.721	37.208
14	13.706	0.136	0.267	1.099	48.324
15	15.767	0.270	0.313	1.121	62.413
16	20.287	0.431	0.392	1.671	66.274

Table 2 also indicates the magnetic disturbance magnitude for each scenario. The categorization was done based on the standard deviation of both the acceleration (STD Acc.) and deviation from the expected magnetic field norm (STD Mag.). The former characterizes the dynamic activity of the motion, as higher variability indicates more abrupt or rapid movements. The latter reflects magnetic disturbances since deviations from the Earth's nominal field suggest local interference or anomalies.

In summary, the most dynamic scenario was clearly Scenario #8, combining high translational and rotational activity. Both Scenarios #1 and #9 reflected the slowest and most spatially constrained motions. Scenario #16 stood out for covering the most distance and operating in the largest volume, indicative of extensive exploration.

The total spatial volume covered across all trajectories was 0.804 m^3. The longest trajectory was observed in Scenario #8, spanning 23.85 meters, while the shortest trajectory occurred in Scenario #9, with a length of 6.53 meters.

The fastest overall motion was recorded in Scenario #16, with an average speed of 0.39 m/s, whereas the slowest movement took place in Scenario #1, averaging only 0.12 m/s. The greatest orientation change was also found in Scenario #8, showing a total RPY rotation of 88.17 rad, and this scenario also exhibited the fastest rotational motion, with an average angular velocity of 0.91 rad/s.

Figure 2 depicts the executed trajectories for four random scenarios; the dynamics of the trajectory is color coded.

Table 2
Characteristics of the executed scenarios based on MARG data

Scen.	Avg. ang. velocity (rad/s)	STD Acc. (m/s^2)	STD Mag. (uT)	Dynamics	Magnetism
1	0.165	0.107	1.823	Low	High
2	0.221	0.214	1.768	Low	Low
3	0.274	0.344	1.762	Low	Low
4	0.421	1.858	1.621	High	Low
5	0.508	1.248	3.708	High	High
6	0.571	2.428	1.804	High	Low
7	0.746	2.878	4.651	High	High
8	0.906	3.284	5.496	High	High
9	0.256	0.222	1.038	Low	Low
10	0.281	0.248	1.032	Low	Low
11	0.362	0.352	1.349	Low	Low
12	0.407	0.474	1.455	Low	Low
13	0.482	2.263	3.916	High	High
14	0.623	2.692	2.770	High	High
15	0.808	2.773	6.994	High	High
16	0.855	2.873	2.871	High	High

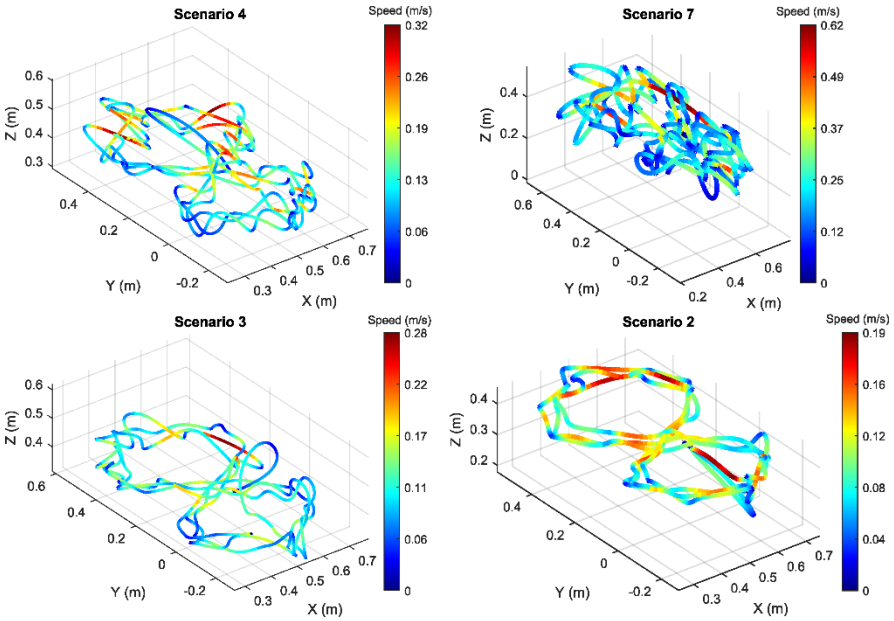

Figure 2
3D trajectories executed by the robot (colored coded by the realized speed magnitude)

4.2 Orientation Estimation Performance

The FFNN-EKF filter performance was evaluated for each scenario and its performance was compared to the standard EKF approach designed based on equations (1)-(4). In the performance evaluation the real orientation $q = \left(q_w, q_x, q_y, q_z\right)^T$ constitutes the ground truth, while the filter outputs the prediction $\hat{q} = \left(\hat{q}_w, \hat{q}_x, \hat{q}_y, \hat{q}_z\right)^T$.

The performance metrics of the sth scenario is given with F_s, while the overall performance is characterized with F:

$$F_s = \frac{1}{N_s}\sum_{k=1}^{N_s}\sqrt{(q_k - \hat{q}_k)^T(q_k - \hat{q}_k)}\,, \quad F = \frac{1}{16}\sum_{s=1}^{16} F_s\,, \tag{7}$$

where s denotes the scenario index ($s = 1,\ldots,16$), N_s is the length the sth scenario (number of samples), while k denotes the sample index.

Figure 3 provides a performance comparison of the standard EKF approach and the proposed FFNN-EKF method. In this evaluation across 16 scenarios, the FFNN-EKF method consistently outperformed the standard EKF, demonstrating significant improvement in estimation accuracy.

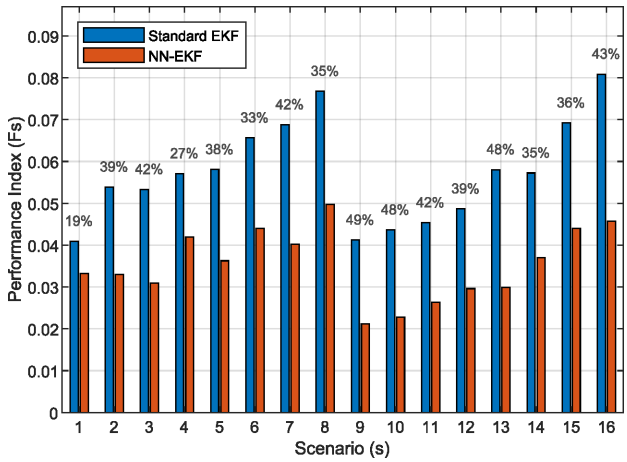

Figure 3
Standard EKF vs FFNN-EKF performance comparison

On average, the performance index of the standard EKF was 0.0551, while the FFNN-EKF achieved a lower (better) average value of 0.0346, indicating significant overall improvement ranging from modest 19% to substantial 49%. The largest performance gain was observed in Scenario #9, where the FFNN-EKF reduced the error by 48.6% compared to the standard EKF. Several other scenarios, such as #3, #7, #10, and #13, also exhibited more than 40% improvement. Even in the worst case (Scenario #1), the NN-EKF still outperformed the standard EKF with a 19.1% improvement.

The aforementioned results strongly suggest that integrating NN-based correction into the EKF framework can significantly enhance estimation performance, especially in complex scenarios.

In low magnetic disturbance scenarios, the FFNN-EKF showed improvements ranging from approximately 27% to 49%, indicating enhanced performance even under nominal conditions. In high magnetic disturbance scenarios, the improvements were significant – up to 48% improvement. This suggests that FFNN-EKF is particularly robust in magnetically noisy environments. Under low dynamic conditions, FFNN-EKF provided reliable enhancements over EKF, with significant error reduction observed in Scenarios #9-#12. In high dynamic scenarios, where fast motion or orientation changes are expected, FFNN-EKF maintained strong performance, showing substantial error reduction (e.g., Scenario #8 and #16).

Despite being tested under simultaneously high dynamics and high magnetic disturbance (Scenarios #5, #7, #8, #13-#16), FFNN-EKF maintained its advantage, suggesting high robustness and adaptability of the NN-enhanced method.

Figure 4 presents the orientation estimation performance of the FFNN-EKF method for a 50-second measurement scenario.

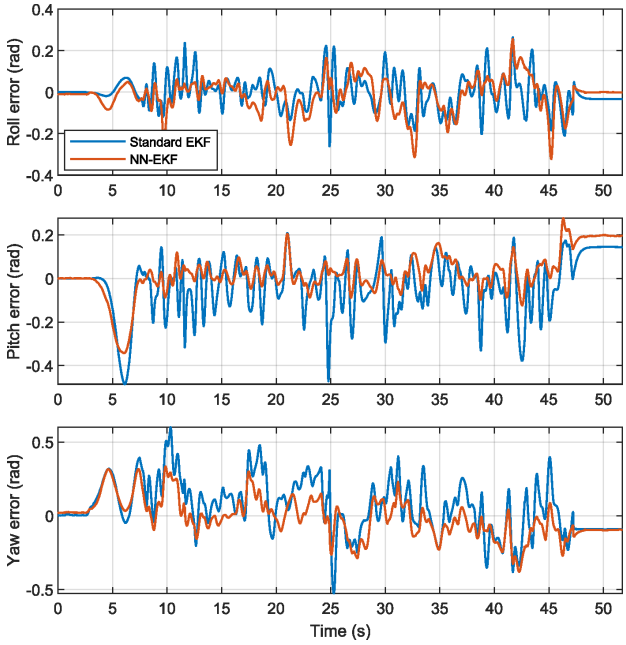

Figure 4
RPY estimation errors of standard EKF and FFNN-EKF approaches

The measurement results highlight the RPY estimation errors with respect to the ground truth for two filtering techniques. The blue lines represent the standard EKF error, while the red lines correspond to the proposed FFNN-EKF approach. It is evident that the FFNN-EKF delivers a marked improvement in estimation accuracy, consistently reducing RPY errors across all axes. This holds true even under challenging conditions involving strong external accelerations or magnetic disturbances. The FFNN-EKF effectively compensates for these disruptions, offering robust and dependable orientation estimates.

Conclusions

This paper evaluated the effectiveness of FFNN-based disturbance estimation and demonstrated the performance gains achieved by integrating the FFNN model into the EKF framework. The proposed disturbance compensator operates on raw magnetometer and accelerometer measurements, as well as an approximated external acceleration vector. It features a single hidden layer with 25 neurons and produces a 6-dimensional output representing the estimated disturbance vectors, which are then used to refine the raw MARG sensor data. The EKF propagates the state using gyroscope measurements and subsequently updates the orientation based on the disturbance-compensated magnetometer and accelerometer observations.

The proposed methodology was validated in a laboratory environment using a UR5 robotic arm equipped with a MARG sensor mounted on its end-effector, following a variety of motion trajectories. Across multiple experimental scenarios, the FFNN-EKF approach consistently outperformed the standard EKF, with orientation estimation accuracy improvements ranging from 19% to 49%. Notably, the method proved to be particularly robust in both magnetically disturbed indoor environments and high-dynamic scenarios typically encountered in outdoor applications such as drone navigation. Future work will focus on deploying the proposed method on mobile robotic platforms, with the aim of evaluating its impact on localization performance in real-world environments.

Acknowledgement

This work was supported by the National Research, Development, and Innovation Fund of Hungary through project no. 142790 under the FK_22 funding scheme.

References

[1] A. Odry, I. Kecskes, R. Pesti, D. Csik, M. Stefanoni, J. Sarosi, and P. Sarcevic: Nn-augmented EKF for robust orientation estimation based on MARG sensors, International Journal of Control, Automation and Systems, 2025, Vol. 23, No. 3, pp. 920-934

[2] L. Somlyai and Z. Vamossy: Improved rgb-d camera-based slam system for mobil robots, Acta Polytechnica Hungarica, 2024, Vol. 21, No. 8, pp. 107-124

[3] X. Xu, Y. Sun, X. Tian, L. Zhou, and Y. Li: A novel orientation determination approach of mobile robot using inertial and magnetic sensors, IEEE Transactions on Industrial Electronics, 2022, Vol. 70, No. 4, pp. 4267-4277

[4] M. Vigne, A. El Khoury, M. Petriaux, F. Di Meglio, and N. Petit: Movie: A velocity-aided imu attitude estimator for observing and controlling multiple deformations on legged robots, IEEE Robotics and Automation Letters, 2022, Vol. 7, No. 2, pp. 3969-3976

[5] H. Son, B. Lee, and S. Sung: Synthetic deep neural network design for lidar-inertial odometry based on cnn and lstm, International Journal of Control, Automation and Systems, 2021, Vol. 19, No. 8, pp. 2859-2868

[6] M. A. Javed, M. Tahir, and K. Ali: Attitude in motion: Constraints aided accurate vehicle orientation tracking in harsh environment, IEEE Transactions on Industrial Informatics, 2022, Vol. 19, No. 5, pp. 6450-6459

[7] L. Wang, S. Xia, H. Xi, S. Li, and L. Wang: Robust visual inertial odometry estimation based on adaptive interactive multiple model al- gorithm, International Journal of Control, Automation and Systems, 2022, Vol. 20, No. 10, pp. 3335-3346

[8] S. Yakupoglu-Altuntas, M. Esit, H. E. Soken, and C. Hajiyev: Backup magnetometer-only attitude estimation algorithm for small satellites, IEEE Sensors Journal, 2022, Vol. 22, No. 13, pp. 13544-13551

[9] N. Ratchatanantakit, O. Nonnarit, P. Sonchan, M. Adjouadi, and A. Barreto: A sensor fusion approach to marg module orientation estimation for a real-time hand tracking application, Information Fusion, 2023, Vol. 90, pp. 298-315

[10] D. Laidig and T. Seel: Vqf: Highly accurate imu orientation estimation with bias estimation and magnetic disturbance rejection, Information Fusion, 2023, Vol. 91, pp. 187-204

[11] J. K. Lee, T. H. Jeon, and W. C. Jung: Constraint-augmented kalman filter for magnetometer-free 3d joint angle determination, International Journal of Control, Automation and Systems, 2020, Vol. 18, No. 11, pp. 2929-2942

[12] M. Caruso, A. M. Sabatini, M. Knaflitz, M. Gazzoni, U. Della Croce, and A. Cereatti: Orientation estimation through magneto-inertial sensor fusion: A heuristic approach for suboptimal parameters tuning, IEEE Sensors Journal, 2020, Vol. 21, No. 3, pp. 3408-3419

[13] B. Candan and H. E. Soken: Robust attitude estimation using imu-only measurements, IEEE Transactions on Instrumentation and Measurement, 2021, Vol. 70, pp. 1-9

[14] G. I. Perez-Soto, K. A. Camarillo-Gomez, J. Rodriguez-Resendiz, and C. G. Manriquez-Padilla: Novel technique to increase the effective workspace of a soft robot, Micromachines, 2024, Vol. 15, No. 2, p. 197

[15] J. R. Garcia-Martinez, J. Rodriguez-Resendiz, and E. E. Cruz-Miguel: A new seven-segment profile algorithm for an open source architecture in a hybrid electronic platform, Electronics, 2019, Vol. 8, No. 6, p. 652

[16] A. Odry, I. Kecskes, D. Csik, H. A. Hashim, and P. Sarcevic: Adaptive gradient-descent extended kalman filter for pose estimation of mobile robots with sparse reference signals, 2022 IEEE/RSJ International Conference on Intelligent Robots and Systems (IROS), 2022, pp. 4010-4017

[17] H. A. Hashim and A. E. Eltoukhy: Landmark and imu data fusion: Systematic convergence geometric nonlinear observer for slam and velocity bias, IEEE Transactions on Intelligent Transportation Systems, 2020, Vol. 23, No. 4, pp. 3292-3301

[18] H. A. Hashim, M. Abouheaf, and M. A. Abido: Geometric stochastic filter with guaranteed performance for autonomous navigation based on imu and feature sensor fusion, Control Engineering Practice, 2021, Vol. 116, p. 104926

[19] Z. Dai and L. Jing: Lightweight extended kalman filter for marg sensors attitude estimation, IEEE Sensors Journal, 2021, Vol. 21, No. 13, pp. 14749-14758

[20] R. V. Vitali, R. S. McGinnis, and N. C. Perkins: Robust error-state kalman filter for estimating imu orientation, IEEE Sensors Journal, 2020, Vol. 21, No. 3, pp. 3561-3569

[21] S. O. Madgwick, S. Wilson, R. Turk, J. Burridge, C. Kapatos, and R. Vaidyanathan: An extended complementary filter for full-body marg orientation estimation, IEEE/ASME Transactions on mechatronics, 2020, Vol. 25, No. 4, pp. 2054-2064

[22] M. Kok and T. B. Schön: A fast and robust algorithm for orientation estimation using inertial sensors, IEEE Signal Processing Letters, 2019, Vol. 26, No. 11, pp. 1673-1677

[23] W. Sun, J. Wu, W. Ding, and S. Duan: A robust indirect kalman filter based on the gradient descent algorithm for attitude estimation during dynamic conditions, IEEE Access, 2020, Vol. 8, pp. 96487-96494

[24] B. Candan and S. Servadio: Relative pose estimation of an uncooperative target with camera marker detection, Aerospace, 2025, Vol. 12, No. 5, p. 425

[25] A. Odry, I. Kecskes, P. Sarcevic, Z. Vizvari, A. Toth, and P. Odry: A novel fuzzy-adaptive extended kalman filter for real-time attitude estimation of mobile robots, Sensors, 2020, Vol. 20, No. 3, p. 803

[26] J. Macdonald, R. Leishman, R. Beard, and T. McLain: Analysis of an improved imu-based observer for multirotor helicopters, Journal of Intelligent & Robotic Systems, 2014, Vol. 74, No. 3, pp. 1049-1061

[27] J. Svacha, J. Paulos, G. Loianno, and V. Kumar: Imu-based inertia estimation for a quadrotor using newton-euler dynamics, IEEE Robotics and Automation Letters, 2020, Vol. 5, No. 3, pp. 3861-3867

[28] M. Brossard, A. Barrau, and S. Bonnabel: Ai-imu dead-reckoning, IEEE Transactions on Intelligent Vehicles, 2020, Vol. 5, No. 4, pp. 585-595

[29] M. Brossard, S. Bonnabel, and A. Barrau: Denoising imu gyroscopes with deep learning for open-loop attitude estimation, IEEE Robotics and Automation Letters, 2020, Vol. 5, No. 3, pp. 4796-4803

[30] W. Liu, D. Caruso, E. Ilg, J. Dong, A. I. Mourikis, K. Daniilidis, V. Kumar, and J. Engel: Tlio: Tight learned inertial odometry, IEEE Robotics and Automation Letters, 2020, Vol. 5, No. 4, pp. 5653-5660

[31] J. P. Silva do Monte Lima, H. Uchiyama, and R.-i. Taniguchi: End-to-end learning framework for imu-based 6-dof odometry, Sensors, 2019, Vol. 19, No. 17, p. 3777

[32] W.-Y. Kim, H.-I. Seo, and D.-H. Seo: Nine-axis imu-based extended inertial odometry neural network, Expert Systems with Applications, 2021, Vol. 178, p. 115075

[33] J. Simon, L. Gogolak, and J. Sarosi: Deep reinforcement learning-assisted teaching strategy for industrial robot manipulator, Applied Sciences, 2024, Vol. 14, No. 23, pp. 2076-3417

[34] J. Simon, L. Gogolak, J. Sarosi, and I. Furstner: Augmented reality based distant maintenance approach, Actuators, 2023, Vol. 12, No. 7, p. 302

[35] R. Pesti, P. Sarcevic, and A. Odry: Artificial neural network-based mems accelerometer array calibration, International Journal of Intelligent Robotics and Applications, 2025, pp. 1-21

[36] F. Markley and J. Crassidis: Fundamentals of Spacecraft Attitude Determination and Control, USA: Springer New York, NY, 2014

[37] J. Palfi: The future of adaptive grids using the kalman filter, for data smoothing and data prediction, Acta Polytechnica Hungarica, 2024, Vol. 21, No. 10, pp. 349-364

[38] J. Kuti and P. Galambos: Modular c++ library for relaxed unscented kalman-filtering, Acta Polytechnica Hungarica, 2024, Vol. 21, No. 10, pp. 57-74